Solid Freeform Fabrication 2019: Proceedings of the 30th Annual International
Solid Freeform Fabrication Symposium – An Additive Manufacturing Conference
Reviewed Paper

A Study of Pore Formation During Single Layer and Multiple Layer Build by Selective Laser Melting

Subin Shrestha, Thomas Starr, Kevin Chou

J.B. Speed School of Engineering
University of Louisville
Louisville, KY 40292

Abstract

In this study, different hatch spacings were used to fabricate single layer and multiple layers, and its effect on porosity was investigated by using microcomputed tomography. The combination of laser power (100 W, 150 W, 175 W, and 195W) and scan speeds (600 mm/s, 800 mm/s, 1000 mm/s and 1200 mm/s) which resulted in the least number of pores were selected from the previous single-track experiment. Six levels of hatch spacings were selected based on the track width to form single and multiple layers: 60%, 70%, 80%, 90%, 120% and 150% of track widths. For the multilayer build, the variation in keyhole porosity within the given window of parameters were found to be attributed to the variation in the hatch spacing. In general, the pore number decreased with increase in hatch spacing from 60% to 90% but increased when hatch spacing further increased from 90% to 120%.

Keywords: Computed tomography; Porosity; Selective laser melting.

1. Introduction

Selective laser melting (SLM) is a powder bed additive manufacturing (AM) process which utilizes metal powder as feedstock material. Powder particles are added layer upon layer, and the selected area is melted with the laser. The layer by layer process enables the fabrication of complex components which are otherwise impossible to be fabricated with a subtractive technique. However, the process may form a different kind of defects such as porosities, part deformation, etc. These defects which are formed during the SLM process should be mitigated to improve the part performance.

Pores in the SLM process generally form due to process parameter settings. High energy density leads to keyhole pores, whereas the use of very low energy density leads to lack of fusion pores [1, 2]. But the energy density may not be enough to characterize the porosity [3]. The track morphology, depth of the melt pool, and pore formation are highly dependent on power than scanning speed for the same energy density [3]. Besides, simulation study has shown that the keyhole pores are formed due to the instability of the keyhole, which depends on the applied power [4].

Keyhole pores and lack of fusion pores contribute differently towards the mechanical behavior of the components [5]. A small number of pores formed due to high energy input is harmless when present up to 1 vol.% whereas the effect of the pore formed by insufficient

energy is significant even if the amount is as low as 1 vol.%. Kasperovich et al. [1] presented the correlation between the process parameters and the types of pores formed during SLM fabrication of Ti-6Al-4V parts. Generally, two types of void defects are present in SLM parts, circular/spherical pores are formed with the excessive energy input, whereas insufficient energy density results in elongated, narrow crack-like voids. Reducing these porosities improve tensile performance [6], fatigue performance [7, 8], and hardness [9]. In addition, it is also important to characterize the pores, as the pore location and pore size are critical to the stress concentration and pores near to the surface are more critical even if they are small in size [10].

A few studies have focused solely on the pore formed during the SLM process. Ponnusamy et al. [11] carried out statistical analysis to investigate the effect of laser power, layer thickness, etc. on porosity. As pores are the internal features, X-ray based studies are suitable for non-destructive analysis of porosity and hold an advantage over destructive porosity analysis [12]. Maskery et al. [13] stressed the importance of CT based study as the statistical quality obtained by the data from CT would not be available my metallography due to the requirement of a large number of micrographs. But, the quality of the data obtained from CT analysis depends on its resolution. Siddique et al. [10] performed both X-ray based pore characterization using a voxel resolution of 4.8 μm to scan the SLM specimen and two-dimensional metallographic study to calculate the porosity. The authors found that porosity calculated by metallographic studies and three-dimensional tomography had no significant difference considering the critical pores. Similarly, Wits et al. [14] explained the difference in pore size measurement between micrograph and CT study. The CT always measured the smaller area, but both optical techniques and CT are influenced by several factors which could lead to the observed diversity. Slotwinski et al. [15] utilized X-ray computed tomography (XRCT) to measure porosity on additively manufactured cobalt-chrome (Co-Cr) samples which helped determine the pore distribution within the sample as well as the pore morphology. In a similar manner, Zhou et al. [16] used Synchrotron radiation micro-CT to observe the defects formed within SLM parts. The authors concluded that micro-CT imaging technique is a feasible method to obtain 3D images of SLM defects accurately. Kim et al. [17] utilized μCT as a feedback mechanism to make improvements on initial designs and Van Bael et al. [18] used XRCT as a feedback mechanism to improve the geometrical and mechanical controllability of selective laser melted Ti-6Al-4V porous structures.

This study uses previous single-track results [3] to design the experiment and investigate the effect of hatch spacing. Hatch spacing is another variable, besides laser power and scan speed, which contribute towards the volumetric energy density. Hatch spacing affects the maximum temperature and heat accumulation [19]. Track variations depending upon the hatch spacing is the inherent phenomena of SLM process[20]. Thijs et al. [21] used hatch spacings of 50 μm, 70 μm and 100 μm, while the width of the single track was 97 μm. The micrograph results showed that small pores are formed with smaller hatch spacing, while with 100 μm hatch spacing, larger elongated pores are formed. Read et al. [22] performed analysis of variance to investigate the individual and interaction effect of laser power, scan speed and hatch spacing on the porosity. Based on the analysis, hatch spacing alone did not affect the porosity, but the interaction between the scan speed and hatch spacing affected the porosity. The combinations of laser power (125 W, 150 W, 175 W, and 195 W) and scan speed (600 mm/s, 800 mm/s, 1000 mm/s and 1200 mm/s) from conduction regime are selected and hatch spacing is calculated based on the percentage of the measured track widths. Six levels of hatch spacings are investigated: 60%,

70%, 80%, 90%, 120% and 150% of track width. Again, micro-CT is used to scan the samples and observe the interior pores. Total pore numbers and volume obtained due to the different parameter settings are compared.

2. Experimental Details

Process Parameters Selection

This study is focused on the effect of hatch spacing on the porosity during the SLM process. The single track experiment was performed at first [3], and the measured track width results are utilized to design the single layer and multilayer experiments. Figure 1 shows a typical example of single-track transverse profile showing the width of the single track. The top bead is identified with CT analysis which enables the measurement of track width, even without the observation of the melt profile formed beneath the surface. Hatch spacing is the gap between two successive laser tracks as shown in Figure 1. A percentage of the single-track width is used to define the hatch spacing and 60%, 70%, 80%, 90%, 120%, and 150% of the track widths are used to form single layer and multilayers. Table 1 lists the laser power, laser speed, track widths from different combination of power and speed, and the corresponding hatch spacing.

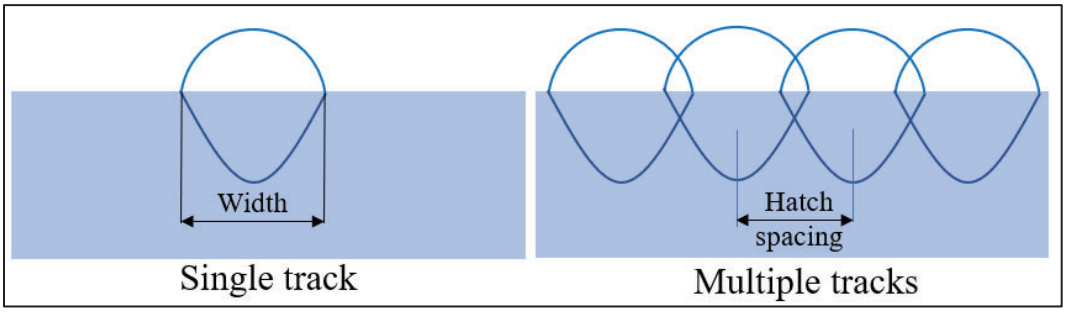

Figure 1: Single track geometry and hatch spacing definition in single layer scanning.

Table 1: Process parameters used in single layer and multilayer design.

Laser power (W)	Scan speed (mm/s)	Track width (μm)	Hatch spacing (μm)					
			60%	70%	80%	90%	120%	150%
125	600	138	83	97	111	124	166	208
125	800	120	72	84	96	108	144	180
125	1000	101	61	71	81	92	122	152
150	600	145	87	102	116	130	174	217
150	800	133	80	94	107	120	160	200
150	1000	121	73	85	97	110	146	182
175	800	143	86	100	115	129	172	215
175	1000	140	84	98	112	126	168	210
175	1200	127	76	91	103	114	152	190
195	800	163	98	114	131	147	196	245

195	1000	155	93	109	125	140	186	232
195	1200	135	81	94	108	121	162	202

Sample Design and Fabrication

Figure 2(a) shows the cylinder design dimensions of the Ti-6Al-4V samples fabricated with EOS M270. The external length and diameter of the cylinder are 18 mm and 7 mm respectively. The micro-CT can scan 13 mm length when using 6 µm pixel size, hence two notches are designed to identify the region containing the test subjects. Each cylinder contains three 3 mm × 3 mm area inside. These areas are formed with different level of hatch spacings. Figure 2(b) shows the cylinder samples after the supports were removed. Figure 3 presents the scan pattern for the single layer and multi-layer builds. For a single layer, X-direction raster scanning is performed, while for multi-layer, alternate X-Y raster scanning is performed. 33 layers with each layer thickness of 30 µm were formed to obtain the multi-layer sample.

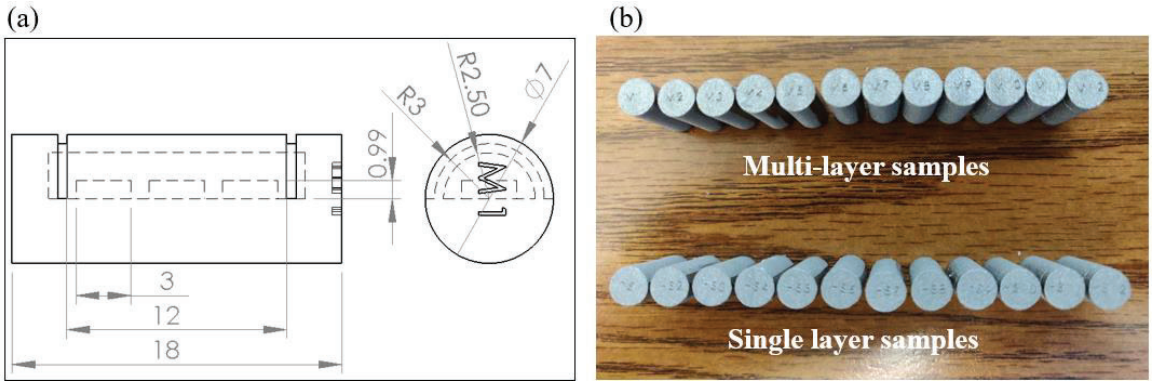

Figure 2: (a) Sample design dimensions and (b) Single layer and multi-layer samples fabricated by EOS M270.

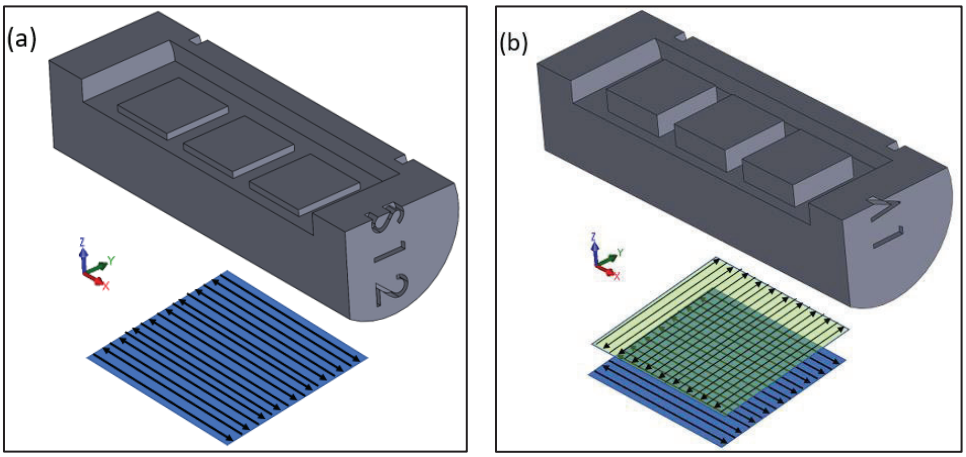

Figure 3: (a) single layer and (b) multi-layer design along with the scan strategies.

3. Results and Discussion

Typical scanning images

The single layer and multilayer samples were scanned using a Bruker 1173 micro-CT scanner, and the data reconstruction and pore analysis explained in the reference [3] is performed. Figure 4 presents the sectional views of single layer sample formed with 150 W and 600 mm/s at different hatch spacings. Three areas on top of the base pad are clearly observed, and the overlap of the track is different for different hatch spacing conditions. Three regions can be identified from the grayscale image: scanned region (light gray), powder region (dark gray) and voids (black). The sectional views of multi-layers, formed with 175 W and 800 mm/s with different hatch spacing of 86 μm, 100 μm, and 115 μm, is also shown in Figure 4.

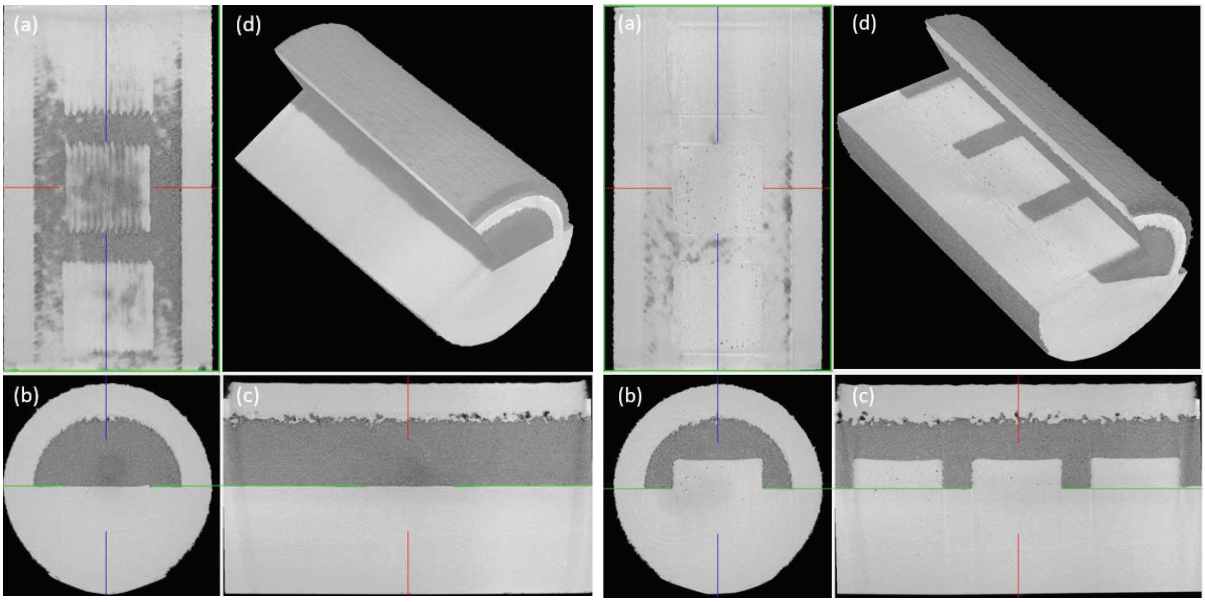

Figure 4: (a) Coronal (X-Z), (b) Transaxial (X-Y), (c) Sagittal (Z-Y) cross-sectional views and (d) partial cut-off view of a single layer and multi-layer.

Single layer experiment results

The single layer surface morphology is shown in Figure 5. The surface is smooth for lower hatch spacing, and the single tracks become more distinct with an increase in hatch spacing. Figure 6 shows the pores formed due to the parameter settings. The parameters were selected based on single track experiment. The average number of pores obtained from three 12 mm long single tracks formed with 125 W and 1000 mm/s is only 0.33, that is one pore was observed in one of the tracks, and two of the tracks did not show any pore. Hence, very few pores are observed in single layer experiment too, as only the pores which are formed below the surface is analyzed and no surface pores were analyzed.

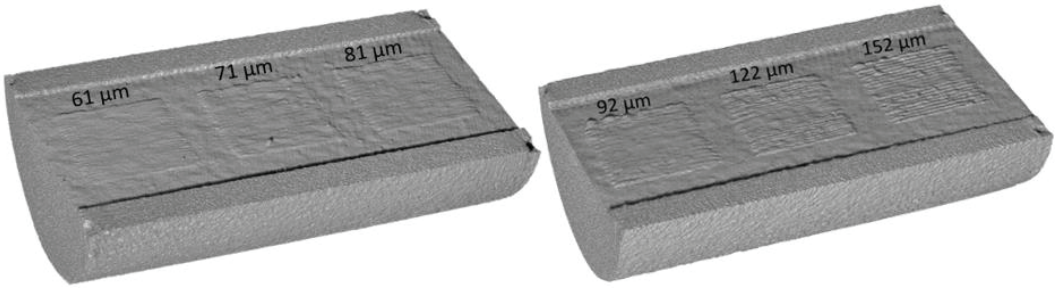

Figure 5: Surface morphologies due to different hatch spacing at 125 W power and 1000 mm/s scan speed.

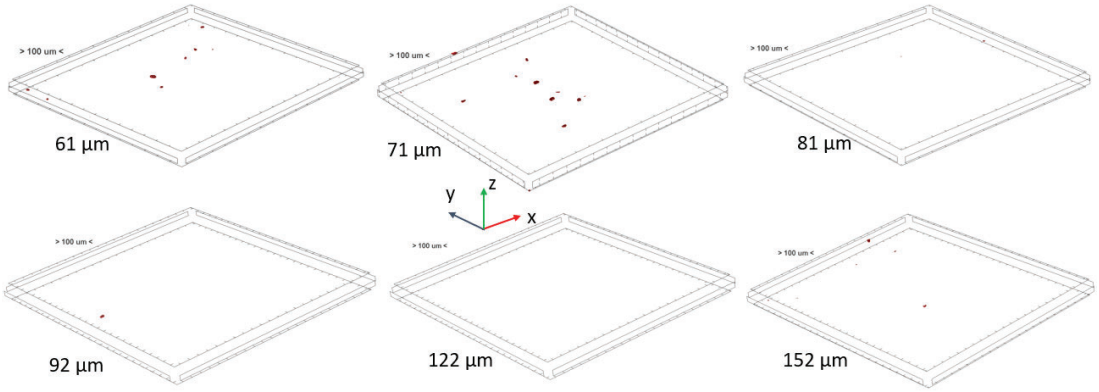

Figure 6: Pore formed due to different hatch spacing at 125 W power and 1000 mm/s scan speed.

Figure 7 shows the pore number obtained from single layers formed with different laser power, scan speed and hatch spacings. Only one sample for each case is analyzed for single-layer samples. No distinct trend is observed from the single layer experiment, mostly due to the limited number of pores being formed. 150 W and 600 m/s, however, resulted in significantly higher number of pores for all hatch spacing compared to other parameters. This may be due to keyhole regime of melting with these parameters. When the pore number is higher, a trend can be observed, that is with increasing hatch spacing, the number of pores mostly decreased. For other cases, hatch spacing did not seem to affect the number of pores during the single layer formation. Besides, the pores may also form due to several other factors like powder spatter formation, etc. which have not been considered in this study.

Higher hatch spacing may lead to lack of fusion pores. Due to the single layer formation, the lack of fusion pores is difficult to identify based on the surface quality. Hence, multilayer fabrication is important to investigate the effect of hatch spacing on the formation of lack of fusion porosity. In addition, 150 W and 600 mm/s case demonstrated that higher number of pores may show some relationship between hatch spacing and the porosity level. The multilayer build is expected to form higher number of pores compared to single layer pores which would help observe the effect of hatch spacing more evidently.

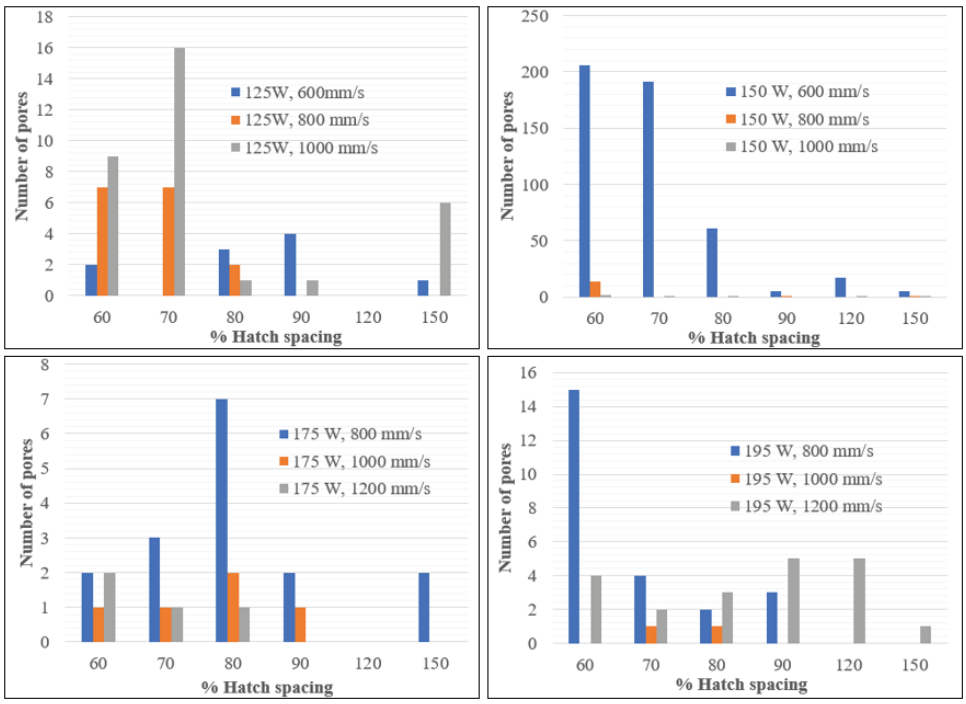

Figure 7: Pore number formed within single layer with different laser parameters

Multiple layer experiment results

The multilayer part formed are shown in Figure 8. The surface with lower hatch spacing has smoother surface which is due to the re-melting of the curved surface formed during single track formation. But, with increase in hatch spacing, the re-melting is insufficient and wavy surfaces are observed. For the hatch spacings greater than track width, individual tracks are identified. Figure 9 shows the pore distribution when 120 % and 150 % hatch spacings are used. A higher number of pores are observed for higher hatch spacing compared to the hatch spacing lower than 100%. The increase in porosity with increase in hatch spacing may be due to the lack of fusion between the tracks. As the hatch spacing of 150% formed a mesh like structure, due to insufficient bonding between the tracks, it is not included in the analysis.

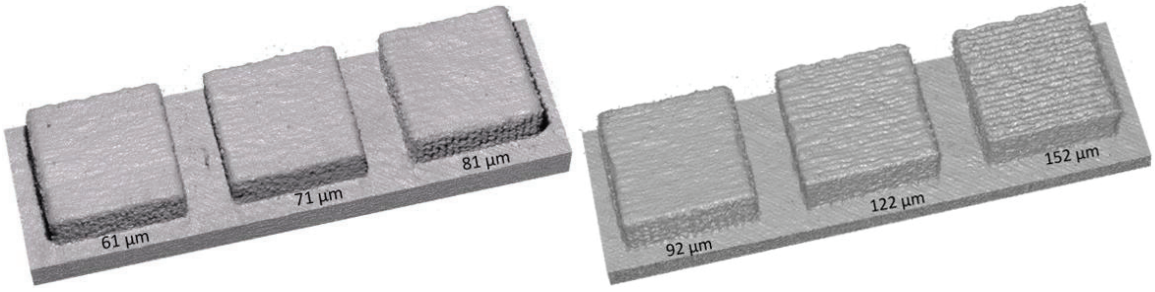

Figure 8: Surface morphologies due to different hatch spacing at 125 W power and 1000 mm/s scan speed

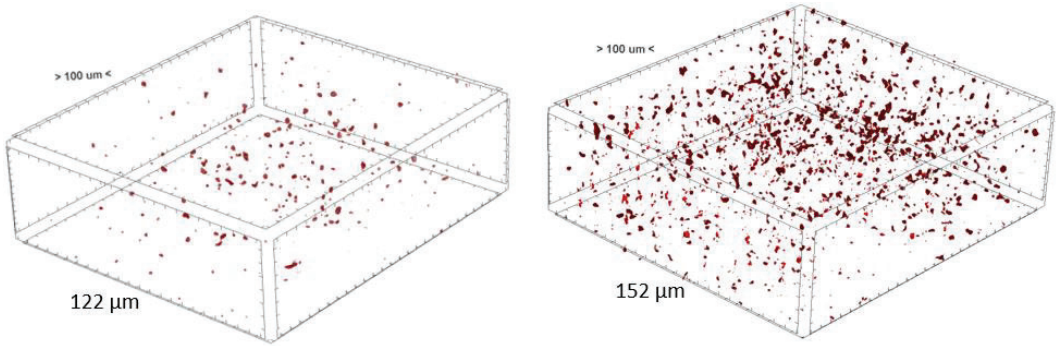

Figure 9: Pores formed due to hatch spacing of 122 µm and 152 µm at 125 W and 1000 mm/s.

Figure 10 presents the average number of pores formed, and standard deviation from three replicates, within the multilayer formed with different process parameters. In general, the pore number decreased with increasing hatch spacing up to 90%, while the pore number increased drastically from 90% to 120%. But, for 195 W, the porosity was minimum when 80% hatch spacing is used. Also, the pore number decreased with decrease in energy density, that is increase in speed for same power and hatch spacing. Although, lower hatch spacing resulted in smoother surface, the higher overlap resulted in higher number of pores. When the hatch spacing is lower, the residual heat may affect the melt pool and at some region keyhole may form resulting to the formation of pores. As the hatch spacing increased from 90% to 120%, the pore number increased significantly. This may be primarily due to the insufficient overlap between the tracks leading to the formation of lack of fusion pores. Figure 9 showed that many elongated pores are formed when 120 % hatch spacing is used except for 150 W and 600 mm/s. This may be due to the variation in track widths formed during successive scanning compared to the single track. During the single-track experiment, only one track is formed, while during the area scanning, residual heat may build up due to successive scanning, leading to wider tracks.

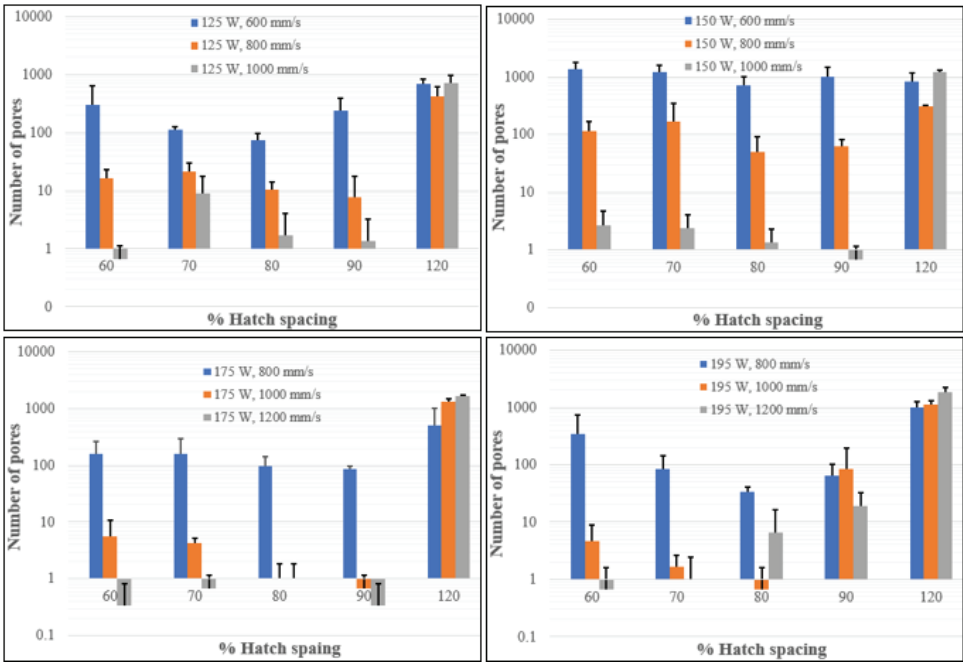

Figure 10: Number of pores formed at different levels of hatch spacing.

Among the parameters tested, 150 W and 600 mm/s resulted in significantly higher number of pores. This is expected as single layer results also show that these parameters lead to higher number of keyhole pores. However, in this case, 120% hatch spacing resulted in fewer number of pores compared to lower hatch spacing, unlike all other set of parameters. Based on the results, porosity can be significantly reduced with proper selection of process parameters for example, 150 W, 1000 mm/s and 90 % (110 µm) hatch spacing.

The volume equivalent diameter of pores is measured and the summary of the average, minimum and maximum pore diameter is presented in Figure 11. There is negligible variation in the average, minimum and maximum pore diameter with respect to hatch spacing for the same power and scan speed. Hence it is observed that the hatch spacing does not affect the size of the keyhole pores. The average pore size decreased with increase in speed for same power as observed in the single-track experiment. 150 W and 1000 mm/s formed negligible or no pore at 80% and 90% hatch spacing. For 150 W, 600 mm/s and 150 W, 800 mm/s, no obvious change in the pore size is observed when hatch spacing increased from 90% to 120%. But, for 150 W and 1000 mm/s, the average pore size increased, and the maximum pore size measured is 77 µm. As the hatch spacing increased, elongated voids may generate due to the insufficient or no overlap between the tracks.

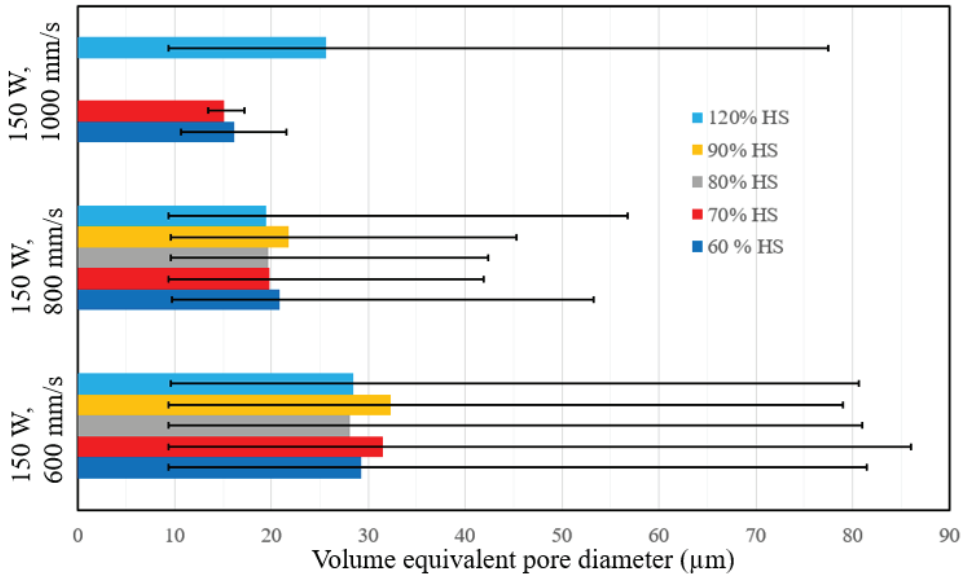

Figure 11: Average pore diameter formed with 150 W at different scan speed and hatch spacings.

4. Conclusions

In this study, single layer and multilayer samples are fabricated with Ti-6Al-4V using EOS M270 to investigate the effect of hatch spacing for different combination of laser power and scan speeds. Three cuboids of 3 mm × 3 mm × 0.99 mm were fabricated within each cylinder sample, and the cylinder samples were scanned using Skyscan 1173 micro-CT scanner to measure the pores formed within. Five levels of hatch spacing, 60%, 70%, 80%, 90%, and 120% of track widths, were analyzed which led to the following conclusions.

- There is no clear effect of hatch spacing on the single-layer build. Less than 10 pores are formed in most of the cases during 3 mm × 3 mm area scanning.
- Multilayer porosity results show that the pore number depend on hatch spacing. The number of pores reduced with increasing hatch spacing up to from 60% to 90%. But the increase in hatch spacing from 90% to 120% introduced lack of fusion pores which significantly increased the pore number.
- The hatch spacing of 60% to 90% did not affect the pore size, while the hatch spacing of 120% introduced lack of fusion pores which increased the average pore diameter.

Acknowledgements

This study is supported by U.S. National Science Foundation under a grant (1662662).

References

1. Kasperovich, G., et al., *Correlation between porosity and processing parameters in TiAl6V4 produced by selective laser melting.* Materials & Design, 2016. **105**: p. 160-170.
2. Panwisawas, C., et al., *On the role of thermal fluid dynamics into the evolution of porosity during selective laser melting.* Scripta Materialia, 2015. **105**: p. 14-17.
3. Shrestha, S., T. Starr, and K. Chou, *A Study of Keyhole Porosity in Selective Laser Melting: Single Track Scanning with Micro-CT Analysis.* Journal of Manufacturing Science and Engineering, 2019: p. 1-23.
4. Shrestha, S. and K. Chou, *A Numerical Study on the Keyhole Formation During Laser Powder Bed Fusion Process.* Journal of Manufacturing Science and Engineering, 2019.
5. Gong, H., et al., *Analysis of defect generation in Ti–6Al–4V parts made using powder bed fusion additive manufacturing processes.* Additive Manufacturing, 2014. **1**: p. 87-98.
6. Galarraga, H., et al., *Effects of the microstructure and porosity on properties of Ti-6Al-4V ELI alloy fabricated by electron beam melting (EBM).* Additive Manufacturing, 2016. **10**: p. 47-57.
7. Leuders, S., et al., *On the mechanical behaviour of titanium alloy TiAl6V4 manufactured by selective laser melting: Fatigue resistance and crack growth performance.* International Journal of Fatigue, 2013. **48**: p. 300-307.
8. Edwards, P. and M. Ramulu, *Fatigue performance evaluation of selective laser melted Ti–6Al–4V.* Materials Science and Engineering: A, 2014. **598**: p. 327-337.
9. Cherry, J., et al., *Investigation into the effect of process parameters on microstructural and physical properties of 316L stainless steel parts by selective laser melting.* The International Journal of Advanced Manufacturing Technology, 2015. **76**(5-8): p. 869-879.
10. Siddique, S., et al., *Computed tomography for characterization of fatigue performance of selective laser melted parts.* Materials & Design, 2015. **83**: p. 661-669.
11. Ponnusamy, P., et al. *Statistical analysis of porosity of 17-4PH alloy processed by selective laser melting*. in *IOP Conference Series: Materials Science and Engineering*. 2017. IOP Publishing.
12. Ziółkowski, G., et al., *Application of X-ray CT method for discontinuity and porosity detection in 316L stainless steel parts produced with SLM technology.* Archives of Civil and Mechanical Engineering, 2014. **14**(4): p. 608-614.

13. Maskery, I., et al., *Quantification and characterisation of porosity in selectively laser melted Al–Si10–Mg using X-ray computed tomography.* Materials Characterization, 2016. **111**: p. 193-204.
14. Wits, W.W., et al., *Porosity testing methods for the quality assessment of selective laser melted parts.* CIRP annals, 2016. **65**(1): p. 201-204.
15. Slotwinski, J.A., E.J. Garboczi, and K.M. Hebenstreit, *Porosity measurements and analysis for metal additive manufacturing process control.* Journal of research of the National Institute of Standards and Technology, 2014. **119**: p. 494.
16. Zhou, X., et al., *3D-imaging of selective laser melting defects in a Co–Cr–Mo alloy by synchrotron radiation micro-CT.* Acta Materialia, 2015. **98**: p. 1-16.
17. Kim, T.B., et al., *Additive manufactured porous titanium structures: Through-process quantification of pore and strut networks.* Journal of Materials Processing Technology, 2014. **214**(11): p. 2706-2715.
18. Van Bael, S., et al., *Micro-CT-based improvement of geometrical and mechanical controllability of selective laser melted Ti6Al4V porous structures.* Materials Science and Engineering: A, 2011. **528**(24): p. 7423-7431.
19. Dong, Z., et al., *Effect of hatch spacing on melt Pool and as-built quality during selective laser melting of stainless steel: modeling and experimental approaches.* Materials, 2019. **12**(1): p. 50.
20. Volpp, J., F. Brueckner, and A.F. Kaplan, *Track geometry variations in selective laser melting processes.* Journal of Laser Applications, 2019. **31**(2): p. 022310.
21. Thijs, L., et al., *A study of the microstructural evolution during selective laser melting of Ti–6Al–4V.* Acta Materialia, 2010. **58**(9): p. 3303-3312.
22. Read, N., et al., *Selective laser melting of AlSi10Mg alloy: Process optimisation and mechanical properties development.* Materials & Design (1980-2015), 2015. **65**: p. 417-424.